Arq. Bras. Med. Vet. Zootec., v.77, n.6, e13558, 2025
http://dx.doi.org/10.1590/1678-4162-13558
Original Article - Veterinary Medicine

Synthesis of Nano-Echinochrome extracted from *Tubipora musica* by *Bacillus amyloliquefaciens* CPFD8, and its potential medical applications as an anti-Alzheimer agent

[*Síntese do Nano-Echinochrome extraído da Tubipora musica pelo Bacillus amyloliquefaciens CPFD8 e suas potenciais aplicações médicas como agente anti-Alzheimer*]

S.A. H. *Hamdi*[1], N.N. *Mostafa*[1], M.F. *Fol*[1], F. *Medhat*[2], I. *Osama*[2], N. *Elsayed*[2], S.H. *Ismail*[3], S.M. *Korany*[4], H. *Sonbol*[4], S. A. Alsaghir[5], M.N.Abd *El-Ghany*[6]*

[1]Zoology Department, Faculty of Science, Cairo University, Giza 12613, Egypt
[2]Biotechnology Department, Faculty of Science, Cairo University, Giza 12613, Egypt
[3]Egypt Nanotechnology Center, Cairo University, El-Sheikh Zayed, Giza, Egypt
[4]Department of Biology, College of Science, Princess Nourah bint Abdulrahman University, P.O. Box 84428, Riyadh 11671, Saudi Arabia
[5]Faculty of Biotechnology, M.S.A University, Cairo, Egypt
[6]Botany and microbiology Department, Faculty of Science, Cairo University, Giza 12613, Egypt

ABSTRACT

Natural products derived from marine organisms have emerged as promising sources of bioactive compounds with potential therapeutic applications. This study aimed to evaluate the antimicrobial, antioxidant, anti-inflammatory, and anti-Alzheimer properties of nano-Echinochrome extracted from the pipe organ coral, *Tubipora musica*. Echinochrome, a red pigment, was extracted biologically using *Bacillus amyloliquefaciens* CPFD8, and its yield was quantified via HPLC analysis. The extracted echinochrome was subjected to ultrasound-assisted green synthesis to produce nanoparticles. Characterization of the nano-echinochrome carried out by X-ray diffraction (XRD), transmission electron microscopy (TEM), scanning electron microscopy (SEM), atomic force microscopy (AFM), dynamic light scattering (DLS), and zeta potential. The antimicrobial assay revealed significant antibacterial effects, particularly against *Staphylococcus aureus*, and moderate antifungal activity against *Aspergillus flavus* as well as significant effects as anti-*Helicobacter pylori*. Additionally, the nano-echinochrome demonstrated substantial antioxidant effects in the DPPH radical scavenging assay and notable anti-inflammatory effects through COX-1/COX-2 inhibition assays. The anti-Alzheimer potential was also demonstrated by significantly inhibiting butyrylcholinesterase (BuChE) enzyme activity. In conclusion, these findings suggest the potential of nano-echinochrome as a multipurpose therapeutic agent capable of attenuating oxidative stress, inflammation, microbial infections, and Alzheimer's disease.

Keywords*:* *Tubípora musica*, *Bacillus amyloliquefaciens* CPFD8, Nano-Echinochrome, Anti-Alzheimer

RESUMO

Os produtos naturais derivados de organismos marinhos surgiram como fontes promissoras de compostos bioativos com potenciais aplicações terapêuticas. Este estudo teve como objetivo avaliar as propriedades antimicrobianas, antioxidantes, anti-inflamatórias e anti-Alzheimer do nano-Echinochrome extraído do coral Tubipora musica. *O Echinochrome, um pigmento vermelho, foi extraído biologicamente usando* Bacillus amyloliquefaciens *CPFD8, e seu rendimento foi quantificado por meio de análise HPLC. O echinochrome extraído foi submetido a síntese verde assistida por ultrassom para produzir nanopartículas. A caracterização do nano-echinochrome foi realizada por difração de raios X (XRD), microscopia eletrônica de transmissão (TEM), microscopia eletrônica de varredura (SEM), microscopia de força atômica (AFM), espalhamento dinâmico de luz (DLS) e potencial zeta. O ensaio antimicrobiano revelou efeitos antibacterianos significativos, particularmente contra* Staphylococcus aureus, *e atividade antifúngica moderada contra* Aspergillus flavus, *bem como efeitos significativos como anti-*Helicobacter pylori. *Além disso, o nano-echinocromo demonstrou efeitos antioxidantes substanciais no ensaio de eliminação de radicais DPPH e efeitos anti-inflamatórios*

---

*Corresponding author: dr.mohamed.naguib@cu.edu.eg
Submitted: April 5, 2025. Accepted: June 17, 2025.

notáveis através de ensaios de inibição de COX-1/COX-2. O potencial anti-Alzheimer também foi demonstrado pela inibição significativa da atividade da enzima butirilcolinesterase (BuChE). Em conclusão, esses achados sugerem o potencial do nano-equinocromo como um agente terapêutico multifuncional capaz de atenuar o estresse oxidativo, a inflamação, as infecções microbianas e a doença de Alzheimer.

Palavras-chave: Tubípora musica, Bacillus amyloliquefaciens *CPFD8, Nano-Echinochrome, Anti-Alzheimer*

INTRODUCTION

Cnidarians provide some of the most significant resources of marine natural products, particularly for the great diversity of bioactive metabolites they produce in their environments (Ghosh *et al*., 2022; Fol *et al*., 2024; Caroll *et al*., 2024). *Tubípora musica*, a species of coral found in tropical and subtropical regions produces a pigment known as (biochrome), these pigments exhibit a wide range of biological activities, including antioxidants, anti-inflammatory, and neuroprotective properties, making them attractive candidates for drug discovery and development (Karthikeyan *et al*., 2022; Rubilar *et al*., 2021; Moodie *et al*., 2019).

Advances in nanotechnology offer exciting opportunities to enhance the therapeutic efficacy and delivery of bioactive compounds, including echinochrome (El-Basiouny *et al*., 2025; Grabacki *et al*., 2022). Nanostructured formulations can improve the solubility, stability, and bioavailability of compounds, enabling targeted delivery to specific tissues or cells (Abd El-Ghany *et al*., 2023a; Tammam and Lamprecht, 2017; Grabacki *et al*., 2022). Furthermore, nanocarriers can facilitate the crossing of biological barriers, such as the blood-brain barrier, thereby enhancing the distribution of therapeutics to the central nervous system (Xie *et al*., 2019).

This research aimed to investigate the synthesis of nano-echinochrome extracted biologically from *Tubípora musica*, its physicochemical characterization, and its potential medical applications as an antimicrobial, anti-*H-pylori*, antioxidant, anti-inflammatory and anti-Alzheimer agent. By leveraging the synergistic effects of nanotechnology and natural products, this study seeks to address the unmet therapeutic needs of natural product nanoparticles and contribute to the development of novel treatment modalities for this devastating disease.

MATERIALS AND METHODS

Organ pipe coral (*Tubípora musica*) was collected from the coastal areas of the Red Sea governorate of Egypt. *Bacillus amyloliquefaciens* CPFD8 was kindly provided by (Abd El-Ghany *et al*., 2023b).

Organ pipe coral was dried in an oven for 10 h at 50°C, then left to complete drying in the open air for 24 h, and finally, ground to a fine powder. The powder was sieved to remove any big particles and then stored in the dark in an airtight container with silica packets at room temperature.

Biological extraction method using *Bacillus amyloliquefaciens* CPFD8 de Man, Rogosa and Sharpe (MRS) media was prepared as follows [MnSO4 0.04gm, peptone from casein 10.0 g, meat extract 8.0 g, tween 80 1.0g, CH3COONa 5.0g, D (+)glucose 20.0g, C6H14N2O7 2.0g, MgSO4 0.2g, yeast extract 4.0g (MERCK)], then 10g of organ pipe coral powder was added to 100 ml of the prepared media, then the media with the powder was autoclaved for 30 minutes at 120 ºC and 1.5 Atm to remove any unwanted microbial organisms. After cooling the media to room temperature, *B. amyloliquefaciens* CPFD8 was inoculated in the autoclaved media in sterilized conditions. Finally, the media was incubated at 35 ºC for 7 days. After incubation the sample was first filtered by filter paper, then it was passed through a 0.45-micro filter to remove any unwanted impurities. This extraction method was adapted from Hamdi *et al*. (2022, 2024a, 2024b, 2025).

The sample was subjected to cooling lyophilization for 72 hours at −45°C and 10 Atm using an “Edwards modulo freeze drier.”

According to Lu *et al*. (2010), this analysis approach was carried out at the National Research Centre in Egypt. An Agilent 1260 series was used for the HPLC analysis. Using an Eclipse C18 column (4.6 mm × 250mm i.e., 5µm), the separation was performed. Methanol: water: Dichloromethane (DCM): acetonitrile (70:4:13:13) (v/v) at a flow rate of 1mL/min made up the mobile phase. An isocratic approach was used to sequentially program the mobile phase. At 280 nm, the diode array detector was observed. The sample solution was injected at a volume of 5µL. At 40 ºC, the column temperature was kept constant.

After dissolving 15-20mg of extract in 1mL of acetone and vortex for 1 minute, the mixture was sonicated for 15 minutes and then filtered through a 0.45µ filter.

Ultrasonic irradiation was utilized to facilitate the synthesis of nanoparticles from the coral species following Peralta-Videa *et al*. (2016). The extract is prepared by dispersing 1gm of organ pipe coral extract in 100mL of double-deionized water. This mixture is then subjected to ultrasonic irradiation using an ultrasonic processor (Heshiler MPS 400, Germany) operating at a frequency of 60 kHz and power output sufficient to maintain a solution temperature not exceeding 70°C. During sonication, ultrasonic waves propagate through the liquid medium, producing alternating high-low-pressure cycles. This created bubbles violently implode during high-pressure cycles, generating localized hotspots with estimated transient temperatures up to 5000 K, pressures above 1000 atm, and heating then cooling rates above 1010 K/s (Flannigan and Suslick, 2010). The collapse of these cavitation bubbles provides the energy required to facilitate chemical reactions involved in nanoparticle synthesis. Hydroxyl and superoxide radicals generated during bubble implosion may also contribute to the reduction of metallic ions and promote the green synthesis of nanoparticles (Makarov *et al*., 2014; Peralta-Videa *et al*., 2016).

A Bruker D8 Discover diffractometer definitively established the crystalline structure and phase purity of the nanoparticles synthesized (Abd El-Samie *et al*., 2025; Tai *et al*. 2010). XRD analysis provides confirmatory evidence that the pure metallic nanoparticles have been successfully obtained through the green reduction process without contamination from unreacted salts or byproducts.

The internal structure and primary particle size distribution were demonstrated using JEOL JEM-2100 (Tumolva *et al*. 2010).

A Thermo Scientific Phenom ProX, produced high-resolution 3D images showing the surface morphology and secondary aggregation state of nanoparticles (Nguyen and Harbison, 2017).

An Agilent 5500 scanning probe system maps surface topology and roughness at the nanoscale (Huang and Andersson, 2013).

DLS analysis revealed the average particle size along with the width of the distribution, indicating the uniformity of nanoparticles generated through the green synthesis process (Stetefeld *et al*., 2016).

A Malvern Zeta-sizer Nano ZSP was used to provide the surface charge and electrokinetic potential of the nanoparticles. The time-dependent changes in hydrodynamic diameter, polydispersity index, and zeta potential can be tracked via periodic DLS and electrophoretic light scattering measurements over days to weeks (Marsalek, 2014; Clogston and Patri, 2010).

To carry out antibacterial effect, the modified diffusion disc technique was applied (Gaydos and Harrington, 1982). This strategy involved culturing 100µL of bacterial or fungal probiotics in fresh media with 10 mL, aiming to achieve around 108 or 105 cells/mL, depending on the probiotics (Pfaller *et al*., 1988). A 100µL probiotics suspension was spread on agar plates and incubated for 48 hours at 25ºC. The fungi used were *Aspergillus flavus*, *Aspergillus niger*, *Candida albicans*, and *Candida parapsilosis*. Amphotericin B was used as a positive control for fungi. Ampicillin, Tetracycline, Gentamicin, and Kanamycin were used as positive controls for Gram-positive bacteria (*Bacillus cereus*, *Bacillus subtilis*, and *Enterococcus faecalis*) and Gram-negative bacteria (*Salmonella typhimrium*, *Staphylococcus aureus*, *Escherichia coli*, *Neisseria gonorrhoeae*, and *Pseudomonas aeruginosa*).To test, 500µL of an organ pipe coral extract was added to the filter disc paper, then it was placed into the agar. The inhibitory zone formed, and its diameter was measured. (Matar *et al*., 2003).

To establish an inoculum of *Helicobacter pylori* strains for susceptibility testing, fresh colonies were transferred into a sterile physiological saline solution and turbidity was corrected to the 0.5 McFarland standard (Clinical and Laboratory Standards Institute, 2006). The suspension created is equivalent to around 1.0 x 10^8 CFU/mL of *H. pylori.* The anti-*Helicobacter pylori* activity was then measured in vitro using the wells agar diffusion method (Castillo-Juárez *et al*., 2007). In summary, 100µL of *H. pylori* suspension (1.0 × 10^8 CFUs/ml) was applied to Mueller Hinton agar plates (BBL) that had 10% sheep blood. Next, using a sterile cork borer or tip, an aseptic hole with a diameter of 6 to 8mm is punched and a 100µL volume of the extracted solution or antimicrobial agent is added to the well. Antibiotics amoxicillin (AMX, 0.05mg/ml), clarithromycin (CLR, 0.05mg/mL), and metronidazole (MTZ, 0.8mg/mL) were utilized as positive controls, while DMSO served as the negative control. The width of the inhibitory zone was measured after a 72-hour incubation period at 37°C in a microaerophilic environment with humidity.

The antioxidant activity assessment was achieved using the 2,2-diphenyl-1-picrylhydrazyl (DPPH) radical scavenging assay (Mahboub *et al*., 2024). Initially, a 0.1mM DPPH solution was prepared by dissolving DPPH in ethanol. The nano-formulated astaxanthin samples were then diluted with ethanol to generate concentrations of 3.9, 7.8, 15.62, 31.25, 62.5, 125, 250, 500, and 1000µg/mL. The ascorbic acid standard was prepared following a similar dilution scheme. Then, 1mL of the prepared DPPH solution was added to 3 ml of the diluted extract solutions, as well as the standard solutions of ascorbic acid. These mixtures were dispensed into triplicate wells of a 96-well plate, and blanks consisting of ethanol only were included for reference. The plate was then incubated at room temperature in the dark for 30 minutes. Following the incubation period, the absorbance of the solutions was measured at 517nm using a Milton Roy UV-VIS microplate spectrophotometer. The percentage of DPPH inhibition was calculated using the formula:

$$\% \text{ DPPH inhibition} = \frac{A0 - A1}{A0} \times 100,$$

where A_0 represents the absorbance of the blank control, and A_1 represents the absorbance of the tested solution.

To assess the antioxidant potency of the samples and standard, a dose-response curve was constructed. The IC_{50} values, representing the concentration at which 50% of the DPPH radical is scavenged, were determined for both the nano-formulated astaxanthin extract samples and the ascorbic acid standard.

To conduct screening for COX-1/COX-2 inhibitors, the following protocol was employed (Blanco *et al*., 1999)

Test inhibitors were dissolved in DMSO and then diluted to 10 times the desired test concentration with COX Assay Buffer before use. Subsequently, 10µL of the diluted test inhibitor or Assay Buffer was added to assigned wells as sample screen [S] or Enzyme Control [EC] (no inhibitor) respectively. For COX-1, 2µL of SC560 and 8µl of COX Assay Buffer were added to one of the wells as Inhibitor Control [IC]. For COX-2, 2µL of Celecoxib and 8µL of COX Assay Buffer were added to one of the wells as Inhibitor Control [IC].

The COX Cofactor was diluted 200 times by adding 2µL of COX Cofactor to 398 µL of COX Assay Buffer immediately before use, ensuring thorough mixing. An Arachidonic acid solution was prepared by combining 5µL of supplied Arachidonic acid with 5µL of NaOH, followed by brief vortexing. This solution was further diluted 10 times by adding 90 µL of ddH_2O and briefly vortexed again. For each well, 80 µL of the master mix was prepared, consisting of 76µl of COX Assay Buffer, 1µL of COX Probe, 2µL of diluted COX Cofactor, and 1µL of COX-1, for the COX-1 reaction, and 1µL of COX-2, for the COX-2 reaction. Subsequently, 80µL of the reaction mixture was added to each well, and 10µL of diluted Arachidonic Acid/NaOH solution was added to each well using a multi-channel pipette to initiate all reactions simultaneously.

To quantify the results, fluorescence was measured kinetically at 25°C for 5-10 minutes, wavelengths of (Ex/Em = 535/587 nm). Two points, T_1 and T_2, were selected within the linear range of the plot, and the corresponding fluorescence values, RFU1 and RFU2, were recorded.

The slope for the sample, including the Enzyme Control (EC), was calculated by dividing the net change in fluorescence (ΔRFU, calculated as RFU2 – RFU1) by the corresponding time interval (ΔT, calculated as T2 – T1). Subsequently, the % Relative Inhibition was determined using the following formula:

$$\% \text{ Relative Inhibition} = \frac{\text{Slope of EC} - \text{Slope of Sample}}{\text{Slope of EC}} \times 100$$

The anti-Alzheimer's activity was evaluated by measuring the inhibition of butyrylcholinesterase (BuChE) enzyme activity following the Ellman method. The hydrolysis of Butyryl thiocholine iodide (BTC) by BuChE was monitored spectrophotometrically in the presence of 5,5'-dithiobis 2-nitrobenzoic acid (DTNB) at 405nm. The reaction mixture contained 50mM MOPS buffer (pH 8), 0.125mM DTNB, and 0.2U/mL BuChE enzyme. The increase in absorbance was monitored for 60 seconds after the addition of BuChE. Two different sample preparations were tested: cooked and direct extract. The samples were tested at various concentrations ranging from 0 to 100µg/mL. The percentage of BuChE inhibition was calculated, and the IC50 value (the concentration required for 50% inhibition) was determined (Miao *et al*., 2022).

RESULTS AND DISCUSSION

Figures 1 and 2 revealed that the concentration of echinochrome extracted from *Tubípora musica* using *B. amyloliquefaciens* CPFD8 is 10µg/g. Comparing our results to those obtained from chemical extraction methods, it is evident that the echinochrome yield from *B. amyloliquefaciens* CPFD8 extraction is significantly lower. For instance, echinochrome chemically extracted using HCl from the shells of *Scaphechinus mirabilis* is 1365.68µg/g (Vasileva *et al*., 2021). Also, using sulfuric acid on the shells of *Diadema setosum* yielded an even higher concentration of 5339.07µg/g (Nhu Hieu *et al*., 2020).

The XRD pattern of organ pipe coral shows a clear diffraction peak at a 2θ angle of 25°, as seen in Fig. 3. This peak suggests that the extract contains crystalline particles.
In the TEM micrographs shown in Fig. 4, the nanoparticles of organ pipe coral appear as discrete, spherical nanostructures with well-defined edges and uniform contrast, indicative of consistent morphology and regular dimensions within the sample.

The sharp circular outlines distinguishable on individual nanoparticles confirm their spherical geometry. Quantitative image analysis of multiple nanoparticles across several TEM images reveals a narrow particle size distribution centered at an average of 19.8 nm diameter, with no significant aggregation or agglomeration. This suggests the green synthesis method can produce spherical metallic nanoparticles of controlled and homogeneous size when optimized. addition, the uniform high contrast across each spherical nanoparticle signifies dense packing of atoms and a crystalline internal structure, which may confer desirable functional properties. The lack of nanoparticles that overlap in the TEM images verifies the effective stabilization of colloidal suspension. This allows for accurate nanomaterial morphology and dimensions characterization through electron microscopy-based techniques.

SEM micrographs as shown in Fig. 5 revealed that the nanoparticles are discernible as discrete, spherical structures with 30-40 nm diameters. Spherical morphology is across all observable particles, indicating high shape uniformity. Furthermore, the particles appear well-separated without significant agglomeration. The distribution shows a narrow, gaussian-like profile centered at 34.2 ± 2.1 nm diameter. This corroborates the uniform particle dimensions qualitatively observed in the SEM images. The spherical geometry and homogeneous size distribution verify the ability of the ultrasound-assisted, extract-based green synthesis method to produce metallic nanoparticles with controlled morphology and dimensions. The discrete nature and lack of aggregation also confirm the effective stabilization of the nanoparticles.

Micrographs of AFM as presented in Fig. 6 demonstrated that the nanoparticles were spherical protrusions rising from the flat substrate surface. Analysis of height profiles across multiple particles shows average heights of 30-35 nm, confirming the spherical nature with dimensions correlating to the diameters determined through electron microscopy. A narrow, gaussian-type distribution is evident, centered at 32.1±1.8nm. Also, size analysis of echinochrome by DLS indicated the formation of spherical nanoparticles with a mean hydrodynamic diameter of approximately 50 nanometers as shown in fig. 7. Zeta potential measurements revealed a highly negative surface charge density of -32 millivolts. The nanoscale size facilitates cellular uptake and extravasation at sites of inflammation or infection, while the strong negative charge confers stability through electrostatic repulsion between particles. These physiochemical properties of ~50 nm size and -32 mV zeta potential endow echinochrome with a high drug encapsulation efficiency and capacity for controlled release, enabling excellent bioactivities.

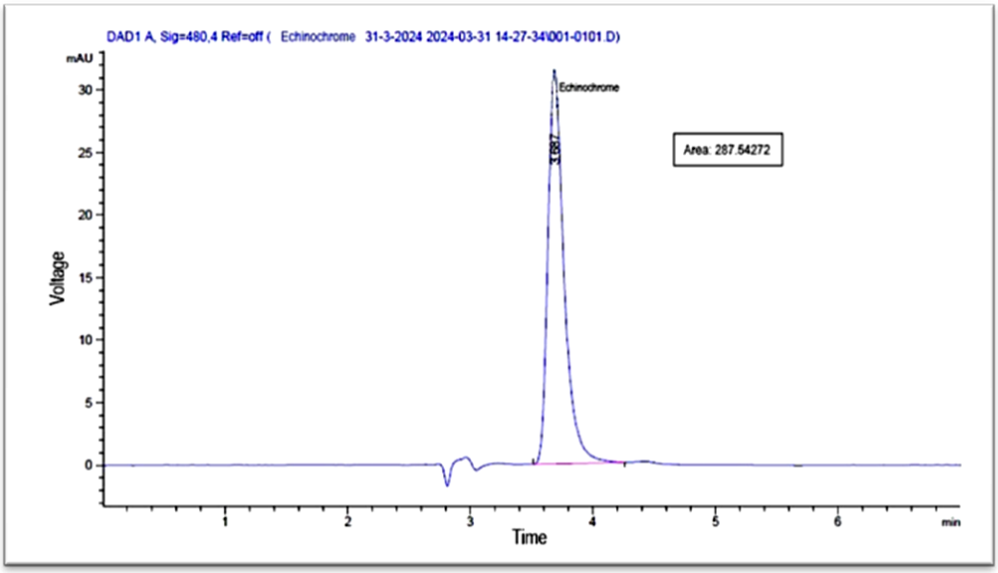

Figure 1. HPLC chromatogram of echinochrome extracted using *B. amyloliquefaciens* CPFD8 from *Tubípora musica*.

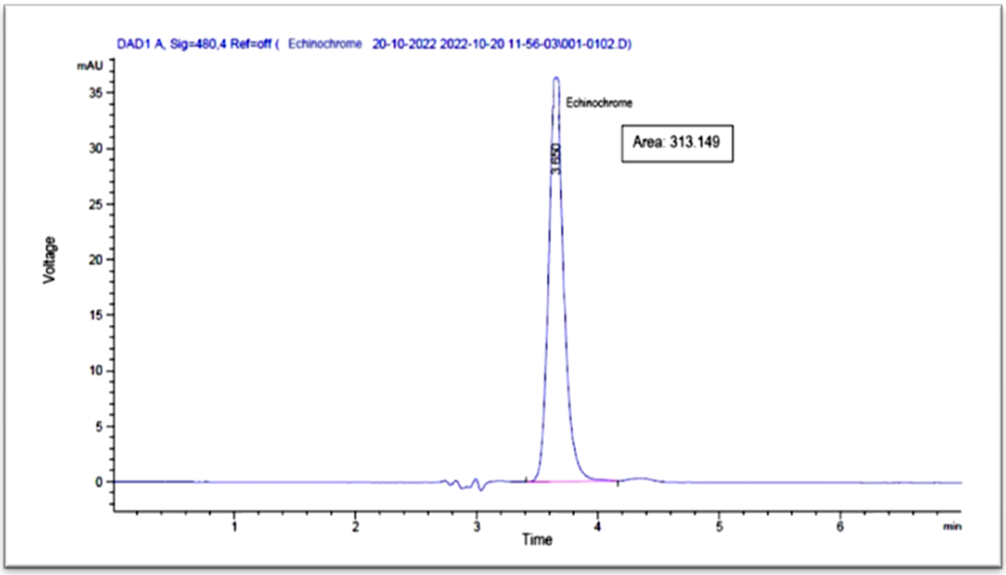

Figure 2. HPLC chromatogram for echinochrome standard solution.

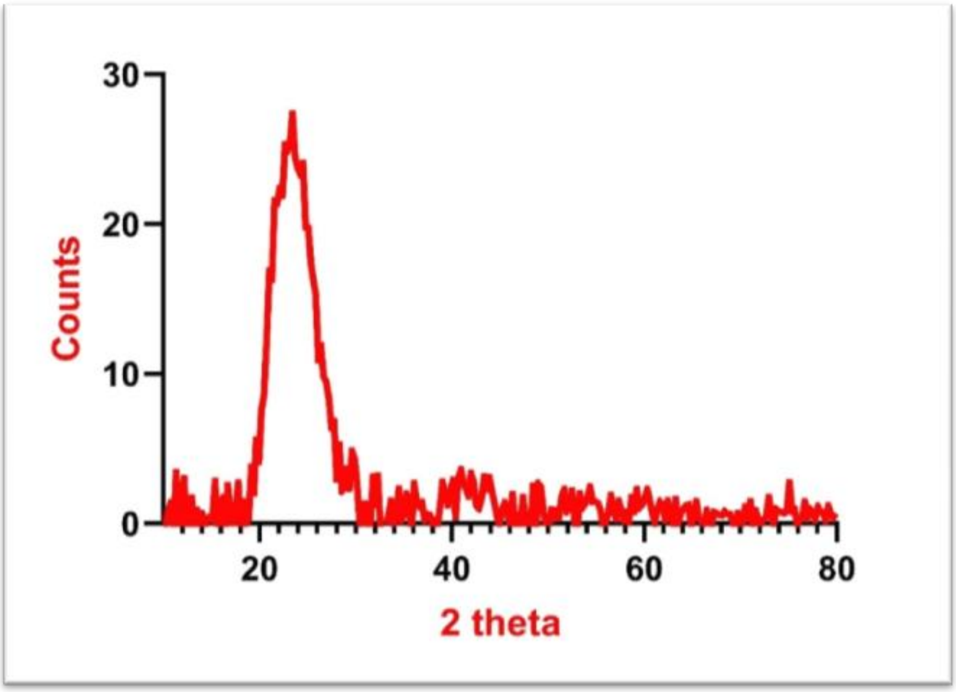

Figure 3. Illustrated the XRD pattern of nano-echinochrome.

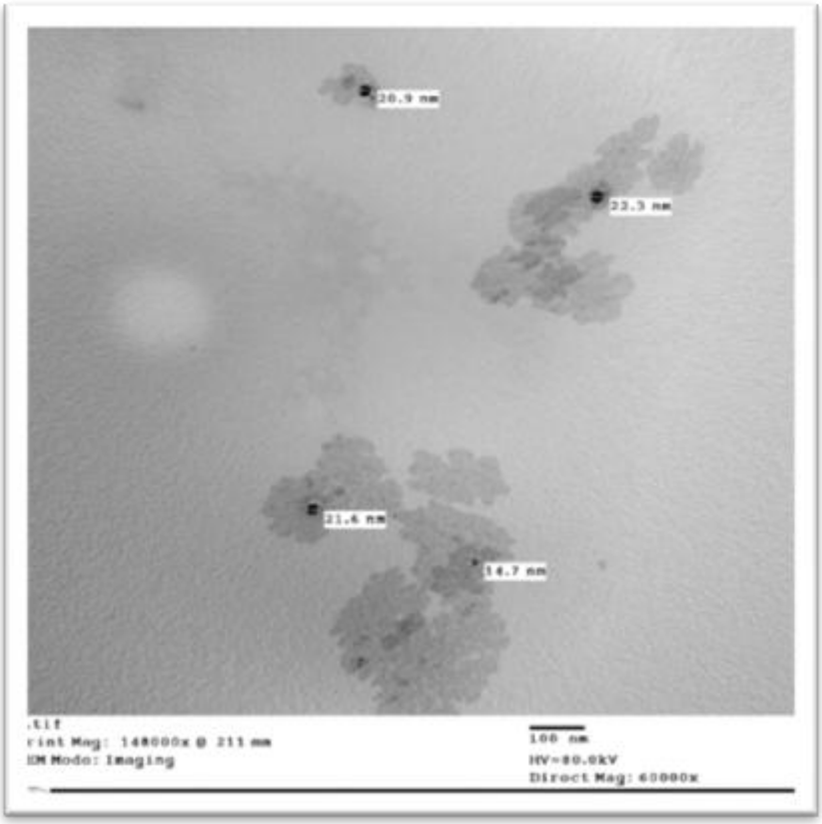

Figure 4. TEM Image of nano-echinochrome.

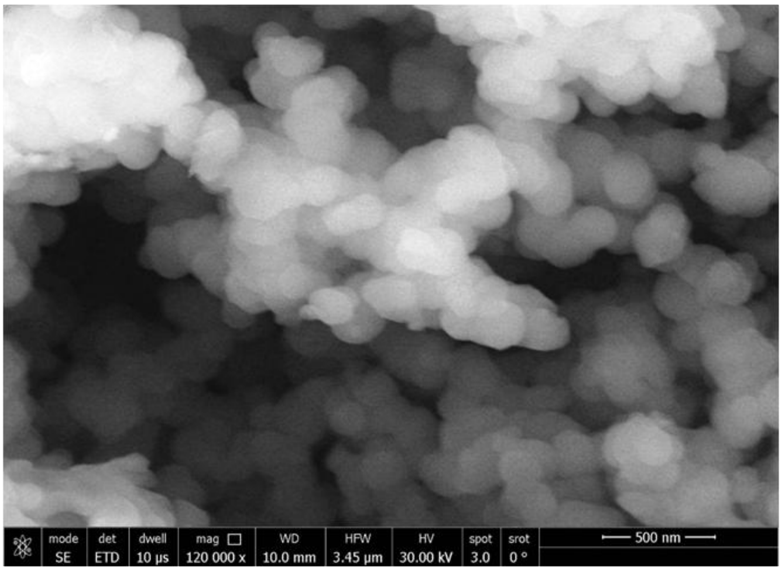

Figure 5. SEM images showing echinochrome nanoparticles.

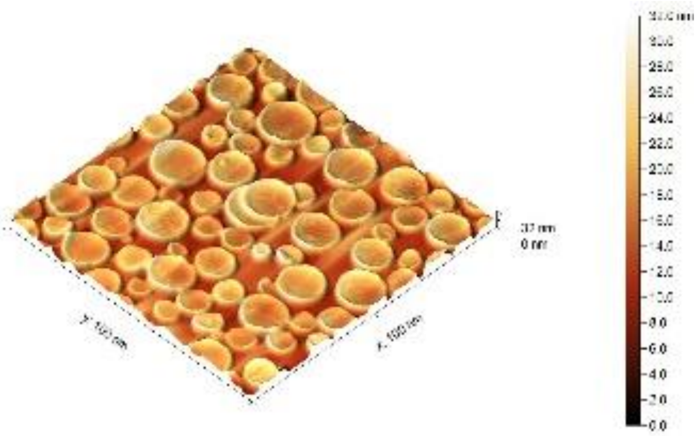

Figure 6 .AFM micrographs of the spherical shape of nano-echinochrome

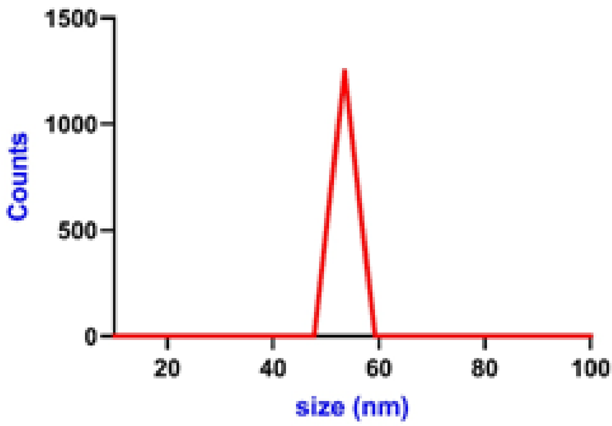

Figure 7. DLS of nano-echinochrome.

The extract showed significant antibacterial activity, with the best inhibition activity against the gram-negative bacteria *Staphylococcus aureus* at 30mm, as shown in Table 1. Also, It showed antifungal activity against *Aspergillus flavus* at 7.5 mm (Table 2). This finding is consistent with Sadek *et al*. (2022). Who found that echinochrome extracted from sea urchins has antibacterial activity against *S. aureus*. Furthermore, the echinochrome extract has antifungal activity against *Aspergillus flavus*. Similarly, Moreno-García *et al*. (2022) reported that echinochrome extracted from *Tripneustes ventricosus* showed 50% inhibition against *C. albicans* and *C. parapsilosis*.

Table 1. The antibacterial activity of nano-echinochrome extracted by the biological method using *B. amyloliquefaciens* CPFD8

Bacterial species	Inhibition zone diameter (mm/10µL Sample)				
	Sample	Standard			
		Ampicillin	Tetracycline	Gentamicin	Kanamycin
Gram-positive					
Bacillus cereus (ATCC:14579)	22	--	28	--	24
Bacillus subtilis (ATCC:6051-)	20	--	34	--	29
Enterococcus faecalis (ATCC:29212)	24	--	30	--	25
Gram negative					
Staphylococcus aureus (ATCC:13565)	30	--	35	--	27
Escherichia coli (ATCC:10536)	28	24	33	--	--
Neisseria gonorrhoeae (ATCC:49226)	25	27	31	--	--
Pseudomonas aeruginosa (ATCC:27853)	24	--	23	18	--
Salmonella typhimrium (ATCC:14028)	28	21	31	--	--

Table 2. The antifungal activity of nano-echinochrome extracted by the biological method using *B. amyloliquefaciens* CPFD8

Fungal species	Inhibition zone diameter (mm / 10µl Sample)	
	Sample	Standard *Amphotericin* B: Antifungal agent
Aspergillus flavus (ATCC:9643)	7.5	20
Aspergillus niger (ATCC:16404)	0	18
Candida albicans (ATCC:10231)	0	22
Candida parapsilosis (ATCC:22019)	0	23

Results showed that the extract had significant activity against *H. pylori* at 27.5 mm compared to the positive control at 24.17mm, as shown in Fig. 8. On the same line, Kang and Kim (2017) and Lee *et al*. (2020) stated that astaxanthin has anti-*Helicobacter pylori* activity.

Results showed that the DPPH Scavenging increased with the concentration of the extract as shown in Fig. 9. The sample's maximum concentration (1000 µg/ml) has a 69.3% DPPH scavenging activity, showing strong antioxidant properties. The IC_{50} value of 53.75 µg/ml indicates that the echinochrome sample may block 50% of DPPH radicals at low concentrations. This suggests that the echinochrome sample has a high antioxidant potency. This is consistent with Halliwell and Gutteridge (2015) and Sennikov *et al*. (2018) who reported that echinochrome's antioxidant action is due to numerous phenolic hydroxyl groups that can donate electrons to destroy free radicals. Also, Popov *et al*. (2020) showed that echinochrome has antioxidant capabilities and could be used to treat oxidative stress-related disorders.

In the present study, it was found that the percentage of inhibition of COX-1 and COX-2 increases as the concentration of the extract increases (Figures 10 and 11). The highest inhibition rate is 112.6% at 500 µg/ml and 83.2% at 1000µg/mL of the extract against COX-1 and COX-2, respectively. The observed reduction of COX-1 and COX-2 enzymes (as shown in fig 12 and 13) shows that echinochrome achieves anti-inflammatory actions via inhibiting prostaglandin synthesis. COX enzymes are essential for converting arachidonic acid into prostaglandins, which are inflammatory solid mediators (Ricciotti and FitzGerald, 2011). The anti-inflammatory activity of echinochrome is consistent with previous studies by Lee *et al*. (2012) who reported that echinochrome has been shown to suppress the expression of inflammatory mediators and cytokines, thereby attenuating inflammation in various experimental models.

The cooked sample's IC_{50} value for BuChE inhibition was 17.12µg/mL. At the highest tested concentration of 100µg/mL, the cooked sample exhibited 87.615% inhibition of BuChE activity. The IC50 value for BuChE inhibition in the direct extract sample was 28.6 µg/mL. At 100µg/mL, the direct extract sample showed 81.477% inhibition of BuChE activity. The results indicate that the cooked and direct extract samples possess anti-Alzheimer's activity by inhibiting the BuChE enzyme. BuChE is a cholinesterase enzyme that hydrolyzes acetylcholine, a neurotransmitter involved in memory and cognitive functions. Inhibition of BuChE can potentially increase the availability of acetylcholine in the brain, which may help alleviate the symptoms of Alzheimer's disease.

The cooked sample exhibited more vital BuChE inhibitory activity than the direct extract, as evidenced by the lower IC_{50} value (17.12µg/mL vs. 28.6µg/mL). This suggests that the cooking process may have enhanced the sample's anti-Alzheimer's potential or altered the composition of active compounds responsible for BuChE inhibition.

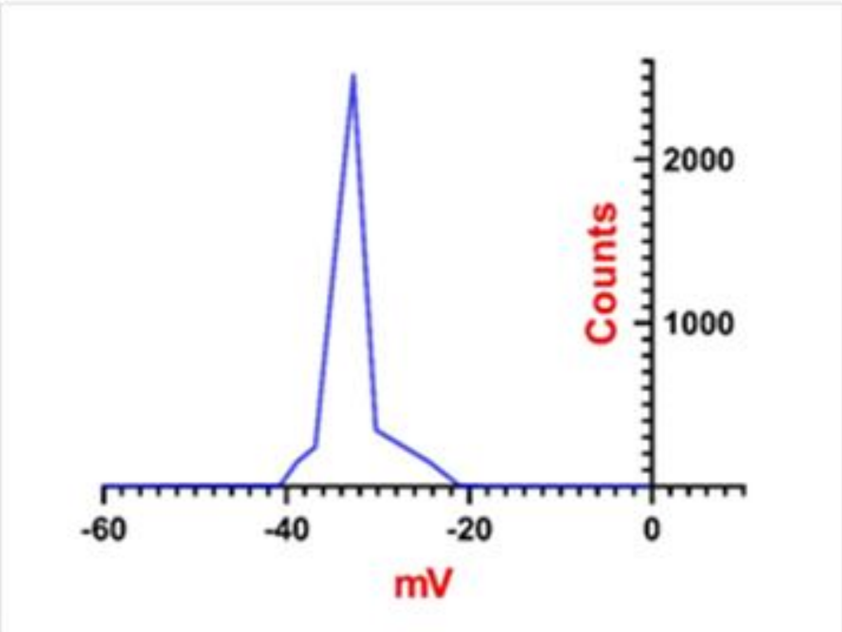

Figure 8. Zeta potential of nano-echinochrome.

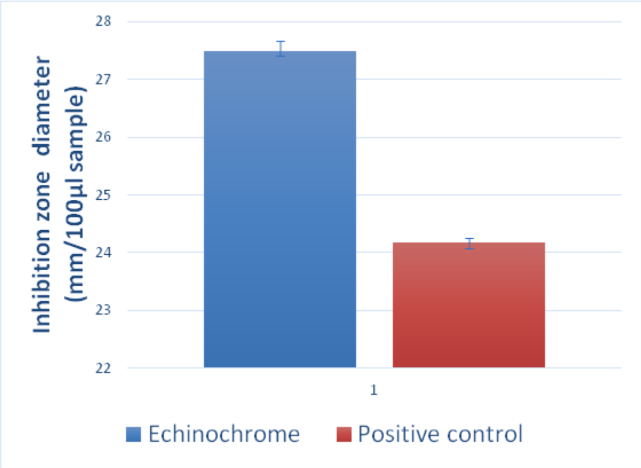

Figure 9. Anti- *Helicobacter pylori* activity of nano-echinochrome extracted by *B. amyloliquefaciens* CPFD8.

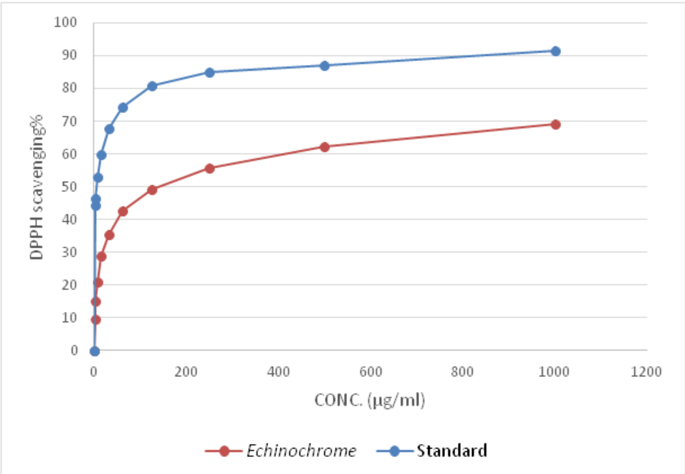

Figure 10. DPPH scavenging activity of nano-echinochrome extracted by the biological method using *B. amyloliquefaciens* CPFD8

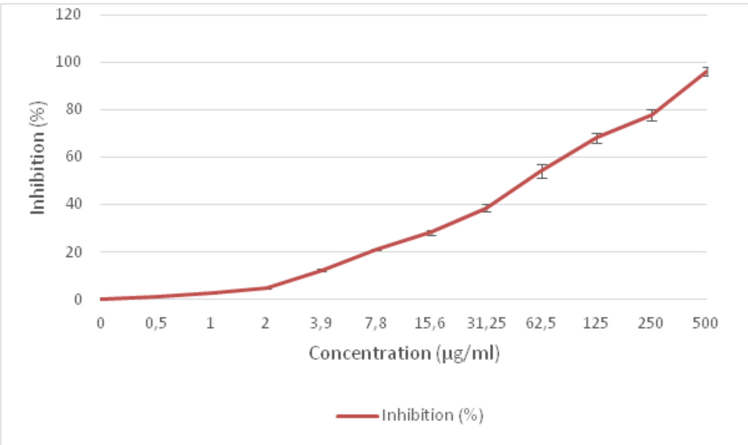

Figure 11. Cox-1 inhibition activity of nano-echinochrome extracted by the biological method using *B. amyloliquefaciens* CPFD8.

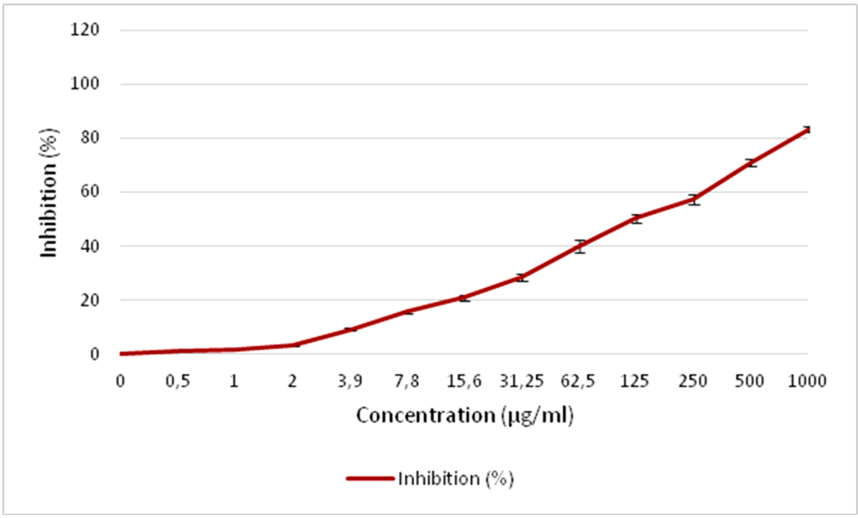

Figure 12. Cox-2 inhibition activity of nano-echinochrome extracted by the biological method using *B. amyloliquefaciens* CPFD8.

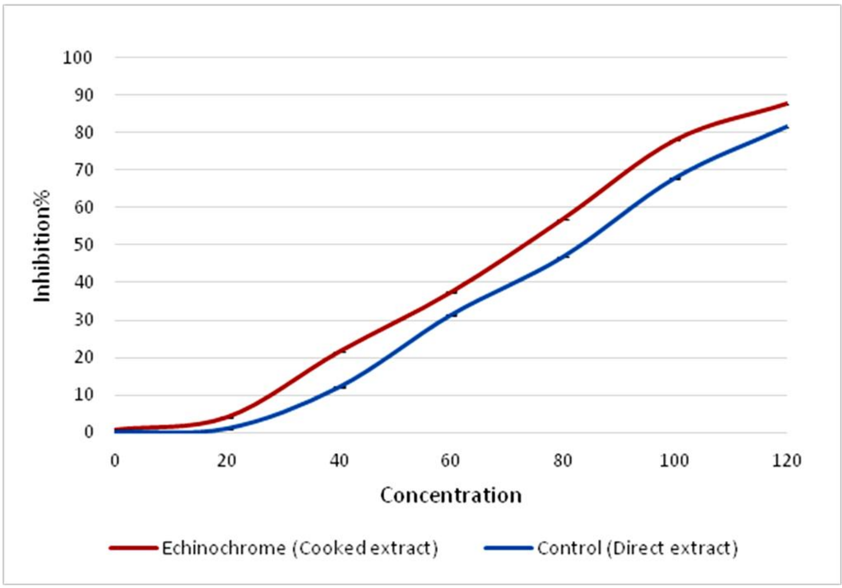

Figure 13. Anti-Alzheimer (butylcholinesterase (BuChE)) inhibition activity of nano-echinochrome extracted using *B. amyloliquefaciens* CPFD8 against control.

CONCLUSION

Using natural marine products combined with nanotechnology offers a promising approach to developing novel therapeutic agents. The current findings indicated that nano-echinochrome exhibits considerable antimicrobial activity against *Staphylococcus aureus*, and anti-fungal activity against *Aspergillus flavus*. Also, the antioxidant and anti-inflammatory properties of echinochrome, combined with nanotechnology, indicate an effect against Alzheimer's disease. This is supported by the observed inhibition of butyrylcholinesterase (BuChE) activity, suggesting its potential as a diverse therapeutic agent. However, further studies, including *in vivo* experiments and clinical trials, should be necessary to confirm the efficacy and safety of these samples as potential anti-Alzheimer agents.

ACKNOWLEDGMENT

Princess Nourah bint Abdulrahman University Researchers Supporting Project number (PNURSP2025R83), Princess Nourah bint Abdulrahman University, Riyadh, Saudi Arabia

REFERENCES

ABD EL-GHANY, M.N., HAMDI, S.A., ELBAZ, R. M. *et al*. Development of a microbial-assisted process for enhanced astaxanthin recovery from crab exoskeleton waste. *Fermentation*, v.9, p.505, 2023**a**.

ABD EL-GHANY, M.N., YAHIA, R.A.; FAHMY, H.A. Nanosensors for agriculture, water, environment, and health. In: GOMAA, A.M.A; CHONG, K.F.; MAKHLOUF, A.S.H. *Handbook of nanosensors*: materials and technological applications. Cham: Springer Nature Switzerland, p.1-29, 2023b.

ABD EL-SAMIE, N.M.; SOLIMAN, S.; KHALIL, N.M.; ABD EL-GHANY, M.N.M. Mycosynthesis of some nanocomposite films using Aspergillus ochraceus NSRN22 for preservation of postharvest lemons. *Egypt. J. Bot*., v.65, p.167-185, 2025.

Blanco, FJ.; Guitian, R.; Moreno, J.; de Toro, FJ.; Galdo, F. Effect of antiinflammatory drugs on COX-1 and COX-2 activity in human articular chondrocytes. J Rheumatol. 1999 26(6):1366-73. PMID: 10381057.

CARROLL, A.R.; COPP, B.R.; DAVIS, R.A.; KEYZERS, R.A.; PRINSEP, M.R. Marine natural products. *Natl. Prod. Rep*., v.41, p.162-207, 2024.

CASTILLO-JUÁREZ, I.; RIVERO-CRUZ, F.; CELIS H.; ROMERO, I. Anti-*Helicobacter pylori* activity of anacardic acids from *Amphipterygium adstringens*. *J. Ethnopharmacol*., v.114, p.72-77, 2007.

CLOGSTON, J.D.; PATRI, A.K. Zeta potential measurement. In: MCNEIL, S.E. (Ed.). *Characterization of nanoparticles intended for drug delivery*. Totowa, NJ: Humana press, 2010. p.63-70.

EL-BASIOUNY, N.M.; SOLIMAN, S.M.; KHALIL, N.M.; ABD EL-GHANY, M.N. Chitosan and alginate/Aspergillus flavus-mediated nanocomposite films for preservation of postharvest tomatoes. *Int. J. Biol. Macromol*., v.297, p.139559, 2025.

FLANNIGAN, D.J., SUSLICK, K.S. Plasma formation and temperature measurement during single-bubble cavitation. *Nature*, v.434, p.52-55, 2010.

FOL, M.; HAMDI, S.; ABDEL RAHMAN, H. *et al*. The protective effect of crawfish chitosan on the reproductive performance of obese male rats. *Food Biosci*., v.57, p.103463, 2024.

GAYDOS, J.M.; HARRINGTON, B.J. Agar disk diffusion for the quality control testing of Autobac elution disks. *Antimicrob. Agents Chemother*., v.21, p.516-518, 1982.

GHOSH, S.; SARKAR, T.; PATI, S.; KARI, Z.A.; EDINUR, H.A. Chakraborty R. Novel bioactive compounds from marine sources as a tool for functional food development. *Front. Mar. Sci*., v.9, p.832957, 2022.

GRABACKI, S.T.; PATHAK, Y.V.; JOSHI, N.H. (Eds.). *Marine-based bioactive compounds*: applications in nutraceuticals. [Florida]: CRC Press, 2022.

HALLIWELL, B.; GUTTERIDGE, J.M.C. *Free radicals in biology and medicine*. Oxford: University Press, 2015.

HAMDI, S.; ELSAYED, N.; ALGAYAR, M. *et al*. Biological extraction, HPLC quantification and medical applications of astaxanthin extracted from crawfish “procambarus clarkii” exoskeleton by-product. *Biology*, v.11, p.1215, 2022.

HAMDI, S.A.; GHONAIM, G.M.; EL SAYED, R.R.; RODRÍGUEZ-COUTO, S.; ABD EL-GHANY, M.N. Bioprocess of astaxanthin extraction from shrimp waste via the common microorganisms Saccharomyces cerevisiae and Lactobacillus acidophilus in comparison to the chemical method. *Biomass Conv. Biorefinery*, v.14, p.8333-8339, 2024a.

HAMDI, S.A.; ZAHRAN, A.K.; ABOU-TALEB, M.A. *et al*. Advances in extraction and biological activities of crawfish chitosan and its application in decolorization of synthetic dyes. *Arq. Bras. Med. Vet. Zootec*., v.76, p.e13250, 2024b.

HAMDI, S.A.H.; ELSAYED, N.; ALGAYAR, M. *et al*. Astaxanthin extraction from lobster “Panulirus penicillatus” waste and its quantification by environmentally safe microbial methods. *Arq. Bras. Med. Vet. Zootec*., v.77, p.e13350, 2025.

HUANG, P.; ANDERSSON, S.B. On detection and estimation in atomic force microscopy at different scan speeds. *IFAC Proc*., v.46, p.153-159, 2013.

KANG, H.; KIM, H. Astaxanthin and β-carotene in *Helicobacter pylori*-induced gastric inflammation: a mini-review on action mechanisms. *J. Cancer Prev*., v.22, p.57-61. 2017.

KARTHIKEYAN, A.; JOSEPH, A.; NAIR, B.G. Promising bioactive compounds from the marine environment and their potential effects on various diseases. *J. Genet. Eng. Biotechnol*., v.20, p.14, 2022.

LEE, H.; LIM, J.W.; KIM, H. Effect of astaxanthin on activation of autophagy and inhibition of apoptosis in *Helicobacter pylori*-infected gastric epithelial cell line AGS. *Nutrients*, v.12, p.1750, 2020.

LEE, S.H.; KO, C.I.; AHN, G.. *et al*. Molecular characteristics and anti-inflammatory activity of the expression of echinoderm microfibrillar-associated protein-like 4 precursors (EMFAL4P) from the sea urchin *Anthocidaris crassispina*. Fish Shellfish Immunol., v.32, p.1201-1208, 2012.

LU, M.; ZHANG, Y.; ZHAO, C.; ZHOU, P.; YU, L. Analysis and Identification of Astaxanthin and its Carotenoid Precursors from Xanthophyllomyces dendrorhous by High-Performance Liquid Chromatography. *Z. Naturforsch. C*, v.65, p.489-494, 2010.

MAHBOUB, H.H.; GAD, W.M.; AZIZ, E.K. *et al*. Silica nanoparticles alleviate the immunosuppression, oxidative stress, biochemical, behavioral, and histopathological alterations induced by *Aeromonas veronii* infection in African catfish (*Clarias gariepinus*). *Fish Physiol. Biochem*., v.50, p.767-783, 2024.

MAKAROV, V.V.; MAKAROVA, S.S.; LOVE, A.J. *et al*. Biosynthesis of nanoparticles using plant extracts. *Nanoscale Res. Lett*., v.9, p.1-8, 2014.

MARSALEK, R. Particle size and zeta potential of ZnO. *APCBEE Proc.*, v.9, p.13-17, 2014.

MATAR, M.J.; OSTROSKY-ZEICHNER, L.; PAETZNICK, V.L. *et al*. Correlation between E-test, disk diffusion, and microdilution methods for antifungal susceptibility testing of fluconazole and voriconazole. *Antimicrob. Agents Chemother*., v.47, p.1647-1651, 2003.

MIAO, S.; HE, Q.; LI, C. *et al.* Aaptamine–a dual acetyl–and butyrylcholinesterase inhibitor as potential anti-Alzheimer's disease agent. *Pharm. Biol*., v.60, p.1502-1510, 2022.

MOODIE, L.W.; SEPČIĆ, K.; TURK, T.; FRANGEŽ, R.; SVENSON, J. Natural cholinesterase inhibitors from marine organisms. *Natl Prod. Rep*., v.36, p.1053-1092, 2019.

MORENO-GARCÍA, D.M., SALAS-ROJAS, M., FERNÁNDEZ-MARTÍNEZ, *et al.* Sea urchins: An update on their pharmacological properties. *Peer J.*, v.10: p.e13606, 2022.

NGUYEN, J.N.T.; HARBISON, A.M. Scanning electron microscopy sample preparation and imaging. *Methods Mol. Biol.*, n.1606, p.71-84, 2017.

NHU HIEU, V.M.; THANH VAN, T.T.; HANG, C.T.T. *et al*. Polyhydroxynaphthoquinone pigment from Vietnam sea urchins as a potential bioactive ingredient in cosmeceuticals. *Natl. Prod. Commun*., v.15, p.1-8, 2020.

PERALTA-VIDEA, J.R.; HUANG, Y.; PARSONS, J.G. *et al*. Plant-based green synthesis of metallic nanoparticles: scientific curiosity or a realistic alternative to chemical synthesis? *Nanotechnol. Environ. Eng*., v.1, p.1-29, 2016.

PFALLER, M.A.; BURMEISTER, L.; BARTLETT, M.S.; RINALDI, M.G. Multicenter evaluation of four methods of yeast inoculum preparation. *J. Clin. Microbiol*., v.26, p.1437-1441, 1988.

POPOV, A.M.; KURKOV, S.V.; AGAPOV, I.I.; POPOVA, G.Y.; SHCHERBAKOV, A.B. 2020 Echinochrome A as a promising agent for prevention and treatment of coronavirus infection (COVID-19). *Biomed. Pharmacother*., v.131, p.110748, 2020.

RICCIOTTI, E.; FITZGERALD, G.A. Prostaglandins and inflammation. *Arterioscl. Thromb.Vasc. Biol.*, v.31, p.986-1000, 2011.

RUBILAR, T.; BARBIERI, E.S.; GAZQUEZ, A.; AVARO, M. Sea urchin pigments: echinochrome A and its potential implication in the cytokine storm syndrome. *Mar. Drugs*, v.19, p.267, 2021.

SADEK, S.A.; HASSANEIN, S.S.; MOHAMED, A.S.; SOLIMAN, A.M.; FAHMY. S.R. Echinochrome pigment extracted from sea urchin suppress the bacterial activity, inflammation, nociception, and oxidative stress resulted in the inhibition of renal injury in septic rats. *J. Food Biochem.*, v.46, p.e13729, 2022.

SENNIKOV, P.G.; PROKOF'EVA, N.G.; KAMENEVA, L.V. Biological activity and prospects for the use of echinochrome. *Pharm. Chem. J*., v.51, p.834-837, 2018.

STETEFELD, J.; MCKENNA, S.A.; PATEL, T.R. Dynamic light scattering: a practical guide and applications in biomedical sciences. *Biophys. Rev*., v.8, p.409-427, 2016.

TAI, F.C.; WEI, C.; CHANG, S.H.; CHEN, W.S. Raman and X-ray diffraction analysis on unburned carbon powder refined from fly ash. *J. Raman Spect*., v.41, p.933-937, 2010.

TAMMAM, S.N.; LAMPRECHT, A. Nanostructures in drug delivery. In: CORNIER, J.; KWADE, A.; VOORDE, M.H.; OWEN, A. (Eds.). *Pharmaceutical nanotechnology*: innovation and production, Weinheim: Wiley-VCH, 2017.

TUMOLVA, L.; PARK, J.Y.; KIM, J.S. *et al*. Morphological and elemental classification of freshly emitted soot particles and atmospheric ultrafine particles using the TEM/EDS. *Aerosol Sci. Technol*., v.44, p.202-215, 2010.

VASILEVA, E.A.; MISHCHENKO, N.P.; TRAN, V.T.; VO, H.M. Fedoreyev SA. Spinochrome identification and quantification in Pacific Sea urchin shells, coelomic fluid and eggs using HPLC-DAD-MS. *Mar. Drugs*, v.19, p.21, 2021.

XIE, J.; SHEN, Z.; ANRAKU, Y.; KATAOKA, K.; CHEN, X. Nanomaterial-based blood-brain-barrier (BBB) crossing strategies. *Biomaterials*, v.224, p.119491, 2019.